Received: 7 February 2022 | Revised: 31 May 2022 | Accepted: 6 June 2022

DOI: 10.1002/cso2.1040

COMPUTATIONAL AND SYSTEMS ONCOLOGY Open Access

WILEY

ORIGINAL ARTICLE

Modeling the role of HIF in the regulation of metabolic key genes LDH and PDH: Emergence of Warburg phenotype

Kévin Spinicci[1,2] | **Pierre Jacquet**[1] | **Gibin Powathil**[2] | **Angélique Stéphanou**[1]

[1]Université Grenoble Alpes, CNRS, UMR 5525, VetAgro Sup, Grenoble INP, TIMC, Grenoble, France

[2]Department of Mathematics, Swansea University, Swansea, UK

Correspondence
Kévin Spinicci, Université Grenoble Alpes, CNRS, UMR 5525, VetAgro Sup, Grenoble INP, TIMC, 38000 Grenoble, France.
Email: 2038726@swansea.ac.uk

Funding information
Centre National de la Recherche Scientifique (MITI interdisciplinary program); Swansea University; IDEX Université Grenoble Alpes

Abstract

Oxygenation of tumors and the effect of hypoxia on cancer cell metabolism is a widely studied subject. Hypoxia-inducible factor (HIF), the main actor in the cell response to hypoxia, represents a potential target in cancer therapy. HIF is involved in many biological processes such as cell proliferation, survival, apoptosis, angiogenesis, iron metabolism, and glucose metabolism. This protein regulates the expressions of lactate dehydrogenase (LDH) and pyruvate dehydrogenase (PDH), both essential for the conversion of pyruvate to be used in aerobic and anaerobic pathways. HIF upregulates LDH, increasing the conversion of pyruvate into lactate which leads to higher secretion of lactic acid by the cell and reduced pH in the microenvironment. HIF indirectly downregulates PDH, decreasing the conversion of pyruvate into acetyl coenzyme A, which leads to reduced usage of the tricarboxylic acid (TCA) cycle in aerobic pathways. Upregulation of HIF may promote the use of anaerobic pathways for energy production even in normal extracellular oxygen conditions. Higher use of glycolysis even in normal oxygen conditions is called the Warburg effect. In this paper, we focus on HIF variations during tumor growth and study, through a mathematical model, its impact on the two metabolic key genes PDH and LDH, to investigate its role in the emergence of the Warburg effect. Mathematical equations describing the enzyme regulation pathways were solved for each cell of the tumor represented in an agent-based model to best capture the spatio-temporal oxygen variations during tumor development caused by cell consumption and reduced diffusion inside the tumor. Simulation results show that reduced HIF degradation in normoxia can induce higher lactic acid production. The emergence of the Warburg effect appears after the first period of hypoxia before oxygen conditions return to a normal level. The results also show that targeting the upregulation of LDH and the downregulation of PDH could be relevant in therapy.

KEYWORDS
hypoxia-inducible factor, metabolism, mathematical modeling, Warburg effect

1 | INTRODUCTION

Cells rely on two main processes to produce ATP: oxidative phosphorylation (OXPHOS) by using oxygen and glycolysis by using glucose. Glycolysis is a pathway generating both ATP and pyruvate using glucose as input [3, 16, 37]. Pyruvate produced by glycolysis can then be used to fuel the tricarboxylic acid (TCA) cycle and produce the compounds involved in OXPHOS, the aerobic pathway. If oxygen is not present, pyruvate is turned into lactate, this process is called fermentation [4]. Lactate formed during fermentation is secreted into the microenvironment, which causes a decrease in extracellular pH.

In 1927, Otto Warburg observed that the tumor consumed more glucose and produced more lactic acid than normal tissues [32]. At first Warburg's observation did not consider the presence of oxygen, yet since increased lactic acid production was also observed when oxygen is available, it has slowly been associated with aerobic glycolysis [14]. Nowadays, a high rate of glycolysis, even if oxygen is available, is known as the Warburg effect [18, 26]. In this paper, we will retain this definition. Tumors can develop anywhere, yet harsh conditions favor tumor appearance [8]. Most tumors have median oxygen levels falling below 2%, the threshold at which the hypoxic response is half-maximal [23]. For this reason, a lot of interest has been put in the effect of oxygenation on tumor metabolism and specifically on the hypoxia-inducible factor (HIF) protein. This protein, being the main actor in the cell response to hypoxia, is interesting to explore as a potential target for cancer therapy since hypoxic cells are more radioresistant [18, 23].

1.1 | HIF structure and mechanism of action

The HIF protein was discovered by Semenza and coworkers during a study on the erythropoietin (EPO) gene, a gene encoding for the erythropoietin hormone involved in red blood cells production, in 1991 [22]. They found DNA sequences in the gene important for its transcriptional activation in hypoxic conditions, now called hypoxia response elements (HRE). The HIF protein is a heterodimer composed of two subunits HIF-1α and HIF-1β, and it acts as a transcription factor by binding to HRE in hypoxic conditions. The subunit HIF-1α is oxygen sensitive and degraded in the presence of oxygen, compared to the constitutively expressed HIF-1β subunit. Three isoforms of the α subunit have been identified: HIF-1α, HIF2-α, and HIF3-α. HIF-1α and HIF2-α are the most studied of the three homologs, HIF-1α is expressed ubiquitously in the body, while HIF2-α expression is tissue specific [22]. It has been demonstrated that overexpression or suppression of HIF-1α or HIF2-α influence each other in vitro and one homolog can be more expressed than the other. Kidney lesions with early Von Hippel-Lindau (VHL) inactivation show more activation of HIF-1α than HIF-2α, but this balance can change [34]. Transcriptional activity of HIF-1α requires the binding of the co-factor CBP/p300 to the C-TAD domain of HIF-1α, then HIF will bind to HRE and activate the transcription of its target genes [12, 17, 22].

1.2 | HIF regulation

Oxygen-dependent regulation of HIF-1α is mainly done by prolyl hydroxylase (PHD) and FIH-1 enzymes. They act at the posttranslational level by inducing its degradation or disrupting its interaction with co-factors. PHD proteins catalyze the hydroxylation of proline residues, targeting HIF-1α for proteasomal degradation by the VHL tumor suppressor protein. Hydroxylation of asparagine residues by factor inhibiting HIF-1 (FIH-1) inhibits the interaction between HIF-1α and the important co-factor CBP/p300, preventing regulation of HIF-1α target genes. Since PHD and FIH-1 need oxygen to hydroxylate HIF-1α residues, they act as oxygen sensors in the cell response to hypoxia. Hypoxia promotes HIF-1α protein stability and transcriptional activity. reactive oxygen species (ROS) and oncometabolites such as succinate, fumarate, and lactate upregulate HIF-1α [12].

Oxygen-independent mechanisms regulating HIF-1α transcription and translation include PI3K/Akt/ mTOR and RAS/RAF/MEK/ERK pathways. Multiple growth factors, oncogenes, mutations (such as in the tumor suppressor genes PTEN and p53), or ROS may increase HIF-1α levels through PI3K and RAS signaling cascade [12, 17, 22]. A study by The Cancer Genome Atlas (TCGA) identified the most altered genes in glioblastoma, it reveals that RTK/RAS/PI3K is among the frequently altered pathways in this disease [24]. It suggests that HIF is a strong candidate for cancer therapy not only because of its role in the cellular response to hypoxia but also of its frequent deregulation in cancer as well. HIF regulation is summarized in Figure 1.

1.3 | Impact on cellular biological functions

The cell response to hypoxia initiated by HIF affects many biological processes such as cell proliferation, survival, apoptosis, angiogenesis, iron metabolism, and glucose metabolism [17]. Pathway enrichment analysis of 98 HIF target genes revealed 20 pathways including

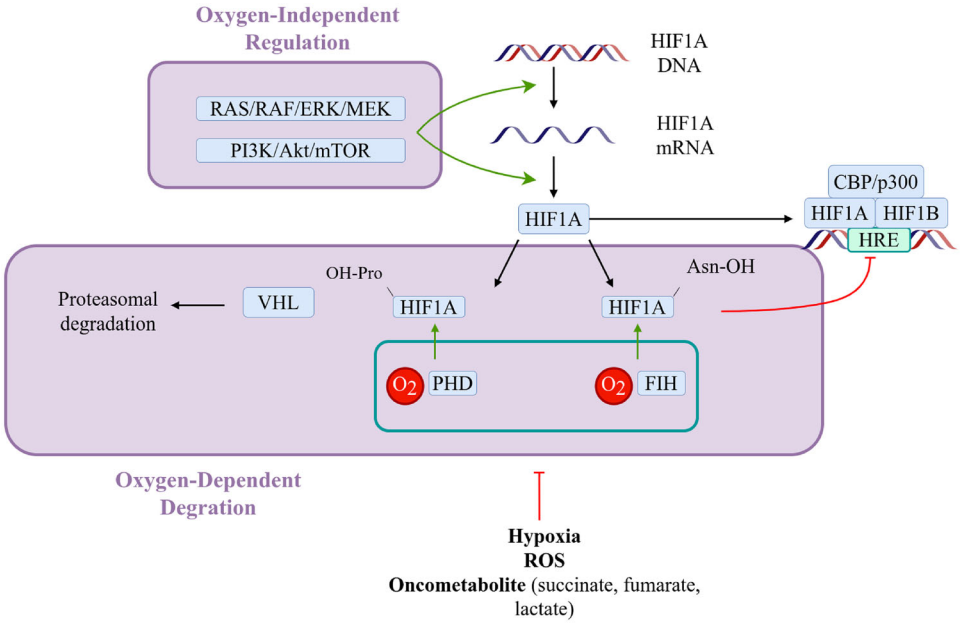

FIGURE 1 Regulation of hypoxia-inducible factor by oxygen-dependent and oxygen-independent mechanisms. PI3K/Akt/mTOR and RAS/RAF/ERK/MEK signaling pathways increase HIF transcription and translation in an oxygen-independent way. The oxygen-dependent regulation relies mainly on the two enzymes: PHD and FIH-1. PHD catalyzes the oxygen-dependent hydroxylation of proline residues on the HIF protein, which is then targeted for proteasomal degradation by the VHL. FIH-1 catalyzes the oxygen-dependent hydroxylation of asparagine residues, which inhibits the interaction between the HIF protein and the CBP/p300 co-factor. Hydroxylation of HIF residues by PHD and FIH-1 is inhibited by hypoxia, ROS, and oncometabolites such as succinate, fumarate, and lactate

those implicated in cancer, glycolysis/gluconeogenesis and metabolism of carbohydrates [27].

HIF can prevent G1/S transition through the regulation of cyclin-dependent kinase inhibitors (p21, p27) and cyclin proteins (cyclin G2, cyclin E) [10]. Cyclin E downregulation is mediated through the inhibition of cyclin D by HIF causing a slowing down or arrest of the cell cycle in the G1 phase and promoting the entry into quiescence, which can be a mechanism to escape chemotherapy [2].

The tricarboxylic acid (TCA) cycle (also called citric acid or Krebs cycle) is a circular process fueled by acetyl-CoA generating NADH and $FADH_2$ for its use in the oxidative phosphorylation (OXPHOS) pathway. Although OXPHOS is the main pathway generating ATP, TCA produces energy in the form of GTP (the equivalent of ATP). These processes represent the aerobic pathways used by the cell when oxygen is present for ATP production. Pyruvate produced by the last steps of the glycolysis is turned into acetyl coenzyme A by pyruvate dehydrogenase (PDH) to fuel the TCA cycle, promoting an oxidative metabolism [4, 36]. However, pyruvate dehydrogenase kinase (PDK) an inhibitor of PDH is upregulated by HIF [19].

When oxygen is not present, the lactate dehydrogenase (LDH) enzyme catalyzes the reaction in which pyruvate formed by the glycolysis is turned into lactate to generate NAD_+. This last step allows glycolysis to continue in anaerobic conditions since NAD_+ is required for pyruvate production. In presence of oxygen, NAD_+ availability is ensured by OXPHOS [4, 36].

Different isoforms of both LDH and PDH enzymes exist. Those isoforms present several differences like kinetics parameters, the tissue, or the cellular compartment where the isoforms are expressed. For example, LDH-A is expressed in the skeletal muscle LDH-B in the heart [21]. LDH-A is also the isoform commonly upregulated in cancer [11]. The differences between isoforms add a level of complexity. However, this is out of the scope of this study.

The Warburg effect is caused by an increase in glucose utilization by the cells, glycolysis being one of the pathways affected by hypoxia. HIF increases the expression of glucose transporters GLUT1 and GLUT3 which contain HRE in their promoters, resulting in higher glucose uptake [13]. Furthermore, HIF induces the overexpression of specific glycolytic isoforms for each enzyme involved in all the steps of the glycolysis [21]. Thus, HIF upregulates the expression of LDH, resulting in higher lactate secretion which acidifies the microenvironment. Not only hypoxia will increase the use of glycolysis by the cell, but it will also reduce the use of the TCA cycle.

In this paper, we want to study how genetic (or epigenetic) regulations, between HIF and its two targets LDH and PDH, may affect the emergence of the Warburg effect. The Warburg effect results in an increased production of

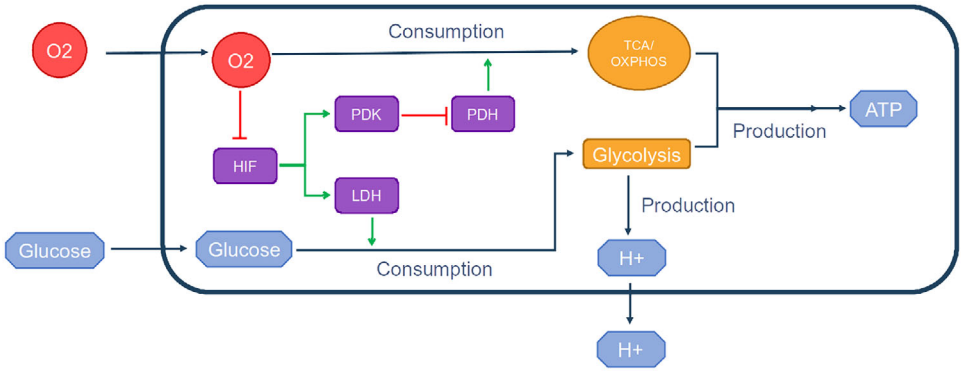

FIGURE 2 Cell metabolism and genetic regulations implemented in the model. Green arrows represent upregulation, and red arrows represent inhibition

lactic acid by the tumor by metabolizing glucose, even in normoxia [7, 15, 18, 26, 28].

2 | MATERIALS AND METHODS

2.1 | Genetic regulations

Here, we assume that HIF plays a major role in mediating the cellular response to hypoxia. We have selected LDH and PDH to model the effect of hypoxia on metabolism since (1) they are key enzymes for the conversion of pyruvate into lactate/acetyl-CoA respectively, after the glycolysis, and (2) they are both regulated by HIF directly or indirectly. PDH is downregulated by HIF through its inhibitor PDK; therefore, PDK will be included in the model (see Figure 2). Genetic regulations are based on the model described by Li et al. [19]. All genetic regulations are described by the following equations:

$$\frac{du}{dt} = A_u - D_u \times H_{O_2 \to u} \times u, \tag{1}$$

$$\frac{dv}{dt} = A_v \times H_{u \to v} - D_v \times v, \tag{2}$$

$$\frac{dw}{dt} = A_w \times H_{u \to w} - D_w \times w, \tag{3}$$

$$\frac{dz}{dt} = A_z \times H_{w \to z} - D_z \times z, \tag{4}$$

where u, v, w, and z are HIF, LDH, PDK, and PDH levels, respectively; A is a parameter for gene production and D for gene degradation. LDH and PDK upregulations by HIF and PDH downregulations by PDK are described with a nonlinear function named the shifted-Hill function. In the same way, the increased HIF protein degradation in normoxia is described using the same function. The shifted-Hill function has the following form:

$$H_{Y \to Z} = \frac{S^n}{S^n + Y^n} + \gamma_{Y \to Z} \frac{Y^n}{S^n + Y^n}. \tag{5}$$

Here, n is the Hill coefficient. S is the gene level with a half-threshold of production. The positive parameter γ represents an activation if > 1 or an inhibition if < 1. $H_{Y \to Z}$ represents the effect of the regulating gene Y on the regulated gene Z, it can be an upregulation if γ is > 1, or a downregulation if γ is < 1. All gene levels are dimensionless, and parameters used in the equation above are summarized in Table 1.

2.2 | Cell metabolism

Nutrient consumption rates change over time depending on microenvironment conditions. In normoxia, glycolysis transforms glucose into pyruvate, then pyruvate is converted to acetyl-CoA by PDH enzymes to feed the TCA cycle. The TCA cycle works in cooperation with OXPHOS to produce ATP using oxygen, which constitutes the aerobic pathway [36]. Since the conversion of pyruvate to acetyl-CoA is catalyzed by the PDH enzyme, its availability bounds the use of TCA and should be reflected in the consumption of oxygen. In hypoxia, glucose consumption is increased to produce the ATP needed using aerobic pathways. Pyruvate formed by glycolysis is then turned into lactate by LDH enzymes, increasing acidity in the microenvironment [36]. Like PDH, increased LDH levels should reflect an increased usage of anaerobic pathways with higher consumption of glucose. As PDH and LDH play an important role in the fate of pyruvate, their respective levels should impact cell metabolism in our model.

In Equations (6) and (7), we define p_O and p_G, two terms to describe the impact of LDH and PDH on glucose and oxygen consumption using a sigmoid function based on

TABLE 1 Parameters used in genetics regulations. The symbol "-" stands for dimensionless

Parameter	Value	Dimension	Parameter	Value	Dimension
A_u	0.05	1/min	D_u	0.005	1/min
A_v	0.005	1/min	D_v	0.005	1/min
A_w	0.005	1/min	D_w	0.005	1/min
A_z	0.005	1/min	D_z	0.005	1/min
$S_{O_2 \to u}$	0.02085	mmol/L	$S_{u \to v}$	4.48	-
$S_{u \to w}$	5.0	-	$S_{w \to z}$	2.2	-
$\gamma_{O_2 \to u}$	10.0	-	$\gamma_{u \to v}$	3.61	-
$\gamma_{u \to w}$	6.97	-	$\gamma_{w \to z}$	0.14	-

the logistic function. p_O and p_G will adjust the consumption rates of oxygen and glucose defined in Equations (8) and (9), by increasing or decreasing the maximal rates according to the level of PDH and LDH.

$$p_O = \frac{\phi_O - \psi_O}{1 + \exp(-l_z(z - z_0))} + \psi_O, \tag{6}$$

$$p_G = \frac{\phi_G - \psi_G}{1 + \exp(-l_v(v - v_0))} + \psi_G. \tag{7}$$

Here, ϕ_O and ϕ_G are the maximal values for p_O and p_G. ψ_O and ψ_G are the minimal values for p_O and p_G. z and v are the current level of PDH and LDH. z_0 and v_0 represent the midpoint of p_O and p_G. l_z and l_v represent the steepness of the curve for p_O and p_G.

Cells consumption and production are described following the functions from the model defined by Robertson-Tessi et al. [25] (a brief description of the complete model is available in the Supporting Information).

Oxygen consumption is determined using a Michaelis–Menten function [25]:

$$f_O = p_O V_O \frac{O_e}{O_e + K_O}. \tag{8}$$

PDH allows the pyruvate to enter the TCA cycle as acetyl coenzyme A, and it is a limiting step in the aerobic pathway. This is included in the model by adjusting the maximum oxygen consumption rate V_O using the term p_O to represent the PDH level effect on metabolism. O_e is the extracellular oxygen concentration. K_O is the extracellular oxygen concentration at which the cell oxygen consumption rate is half-maximum.

Following Robertson-Tessi et al. [25], we assume that ATP demand drives glucose consumption. In low-oxygen conditions, the cell will consume more glucose to produce ATP in the last step of the glycolysis, then pyruvate is turned into lactate by the LDH enzyme. An increase in LDH indicates an upregulation of anaerobic pathways, which means here an increase in glucose consumption. We use the term p_G to increase glucose consumption in Equation (9) when levels of LDH increase [25].

$$f_G = \left(\frac{p_G A_0}{2} - \frac{29 f_O}{10}\right) \frac{G_e}{G_e + K_G}, \tag{9}$$

where A_0 is the target ATP production. G_e is the extracellular glucose concentration. K_G is the extracellular glucose concentration at which the glucose consumption rate is half-maximal.

In this paper, we are studying how HIF can impact the interplay between aerobic (TCA + OXPHOS) and anaerobic (glycolysis + lactate secretion) pathways to generate ATP, due to its PDH and LDH enzymes important for the conversion of pyruvate. Therefore, we do not directly model aerobic and anaerobic pathways but rather we compute the theoretical level of ATP generated by both processes (Equation 12). We take the same stoichiometric coefficients as in [25]: glycolysis uses 1 mol of glucose to produce 2 mol of ATP; the aerobic pathway uses 1 mol of glucose and 5 mol of oxygen to produce 29 mol of ATP. We can compute the ATP produced from the nutrients consumed using the yield from glycolysis and aerobic pathway [25]:

$$f_A = 2 f_G + \frac{29 f_O}{5} \tag{10}$$

Glycolysis produces 2 mol of pyruvate with 1 mol of glucose. If oxygen is absent, pyruvate is turned into lactate, giving a total of 2 mol of lactate [4]. Lactic acid production is given by the glucose consumed:

$$f_{H^+} = k_H 2 f_G, \tag{11}$$

where k_H is a fixed parameter for proton buffering (dimensionless).

The quantity of ATP produced by the cell is modeled by an ODE, and extracellular quantities of the three

molecules oxygen (O), glucose (G), and protons (H^+) are described by PDEs in the following equations:

$$\frac{dA}{dt} = f_A, \tag{12}$$

$$\frac{\partial O}{\partial t} = D_O \nabla^2 O - \sum_{k=1}^{N_i} f_O^k, \tag{13}$$

$$\frac{\partial G}{\partial t} = D_G \nabla^2 G - \sum_{k=1}^{N_i} f_G^k, \tag{14}$$

$$\frac{\partial H^+}{\partial t} = D_{H^+} \nabla^2 H^+ + \sum_{k=1}^{N_i} f_{H^+}^k, \tag{15}$$

where D_O, D_G, and D_{H^+} are the diffusion coefficient for each molecule. N_i is the number of cells in the voxel i. Initial values for oxygen in Equation (13) are $O(x, y, 0) = 0.056$ mmol/L in normoxia and 0.012 mmol/L in hypoxia. The initial value for glucose in Equation (14) is $G(x, y, 0) = 5.0$ mmol/L. The initial value for protons in Equation (15) is $H^+(x, y, 0) = 3.98 \times 10^{-5}$ mmol/L (pH 7.4). Let x_0 and y_0 be the lower boundary of the domain in x and y and x_L and y_L be the upper boundary in x and y. Boundary values for oxygen in Equation (13) are $O(x_0, y, t) = O(x_L, y, t) = O(x, y_0, t) = O(x, y_L, t) = 0.056$ mmol/L in normoxia and 0.012 mmol/L in hypoxia. Boundary values for glucose in Equation (14) are $G(x_0, y, t) = G(x_L, y, t) = G(x, y_0, t) = G(x, y_L, t) = 5.0$ mmol/L. Boundary values for H^+ in Equation 15 are $H^+(x_0, y, t) = H^+(x_L, y, t) = H^+(x, y_0, t) = H^+(x, y_L, t) = 3.98 \times 10^{-5}$ mmol/L (pH 7.4). Parameters used in these functions are summarized in Table 2. The schematic in Figure 2 shows the cellular metabolism and the genetic regulation implemented in the model.

TABLE 2 Parameters for metabolism. The symbol "-" stands for dimensionless

Parameter	Value	Unit
V_O	0.01875	mmol/L/min
K_O	0.0075	mmol/L
K_G	0.04	mmol/L
k_H	2.5e-4	-
A0	0.10875	mmol/L/min
ϕ_G	50	-
ψ_G	1	-
l_G	4	-
v_0	2.35	-
ϕ_O	1	-
ψ_O	0	-
l_O	15	-
z_0	0.575	-
D_O	109,200	μ m^2/min
D_G	30,000	μ m^2/min
D_{H^+}	27,0000	μ m^2/min

2.3 | Numerical implementation

The tumor microenvironment plays a vital role in the growth and progression of tumor cells. As the tumor grows, intracellular and intercellular interactions influence the changes in its microenvironment, which can further result in cells dynamic. Here, we aim to develop a modeling framework to simulate the growth of a large population of cells cultured in vitro, each cell having its metabolism influenced by the microenvironment conditions to represent accurately the resource dynamics in the tumor. Therefore, the numerical implementation of the model must have sufficient performance to simulate the behavior of thousands of cells. In this regard, we selected PhysiCell, an open-source C++ framework designed to run simulations containing a large population of cells. This framework has good performance with a low memory footprint, allows the user to implement his custom code and defines custom cell types, and runs a multiagent-based simulation in two or three dimensions [9].

Most aspects of the model are handled by the PhysiCell software [9], this includes cell division and progression through the cell cycle, cell adhesion and repulsion, substrate diffusion, and cell exchanges with the environment (secretion and consumption). Cells are modeled with the shape of a sphere that cannot deform; adhesion and repulsion are implemented using a potential function. The cell division process is implemented as a cycle, where the user can define each step and progress between them. There is no condition in the neighborhood, a cell will divide even if it is surrounded by other cells as long as there are sufficient nutrients. As a consequence, certain regions of the tumor will exhibit a higher cell density. We implemented in PhysiCell a heterogeneous diffusion with respect to local cellular density. In the model, phase duration is 5 h in G1, 8 h in S, 4 h in G2, and 1 h in M, for a total of 18 h to complete a cell cycle [6].

Here, the impact of extracellular oxygen concentration is studied considering different boundary conditions: physiological normoxia at 0.056 mmol/L (5% O_2), pathological hypoxia at 0.01112 mmol/L (1% O_2), and a last where boundary conditions are modified during the simulation from physiological normoxia to pathological hypoxia. The hypoxia threshold is set at 0.02085 (2% O_2), the level at which HIF has a half-maximal response [23].

The governing ODEs (Equations 1–4 and 12) and PDEs (Equations 13–15) are run at each timestep to compute cell

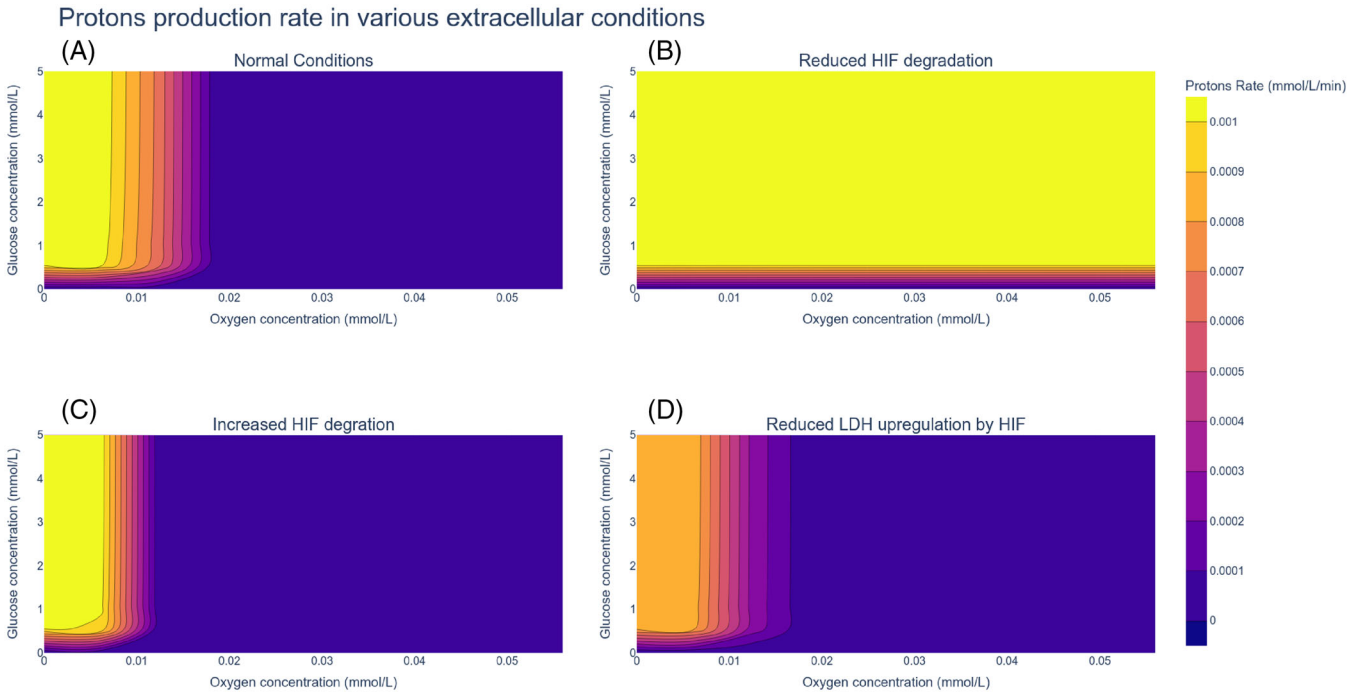

FIGURE 3 Influence of genetic upregulation or inhibition on the production rate of protons at different glucose and oxygen concentrations. (A) Result in no genetic deregulation ($\gamma_{O_2 \to u} = 10.0, \gamma_{u \to v} = 3.61, \gamma_{u \to w} = 6.97, \gamma_{w \to z} = 0.14$). (B) Result with inhibition of the oxygen-dependaet degradation of HIF ($\gamma_{O_2 \to u} = 1.0, \gamma_{u \to v} = 3.61, \gamma_{u \to w} = 6.97, \gamma_{w \to z} = 0.14$). (C) Result with overdegradation of HIF by oxygen ($\gamma_{O_2 \to u} = 40.0, \gamma_{u \to v} = 3.61, \gamma_{u \to w} = 6.97, \gamma_{w \to z} = 0.14$). (D) Result with loss of upregulation of LDH by HIF ($\gamma_{O_2 \to u} = 10.0, \gamma_{u \to v} = 3.0, \gamma_{u \to w} = 6.97, \gamma_{w \to z} = 0.14$)

nutrient consumption, energy, and acidity production for that period. After each time step, the cell state is updated according to the quantity of ATP generated and the extracellular pH. Therefore, cells can proliferate and divide only if they were able to generate enough ATP and if extracellular pH is higher than the acid resistance of the cell (6.1 [25]). If the quantity of ATP generated is less than a threshold $\text{ATP}_{\text{quiescence}}$, the cell enters quiescence and is then prevented to complete the G1 phase. If the quantity of ATP generated is less than a threshold $\text{ATP}_{\text{death}}$ or if the pH is less than a threshold pH_{death}, the cell dies and enters into the death cycle where it is progressively removed from the microenvironment by lysis.

To simulate the cell entry into quiescence, we created a phase G0 with a reversible link to the G1 phase of the cell cycle. If the condition for proliferation are not met, we set the transition rate from G1 to G0 at a maximum value and the rate from G0 to G1 at 0. The cell is forced to enter the G0 phase and is prevented from transit to the G1 phase to continue its division. Once the level of ATP rises again, we revert the transition rate values to allow the cell to leave the G0 phase and divide anew. The cell can only transit to the G0 phase from the G1 phase, thus it will complete its cycle once it leaves the G1 phase and will divide even if ATP levels fall while the division process is ongoing.

3 | RESULTS

3.1 | Qualitative exploration of the model at the cell scale

A well-known phenomenon is the Warburg effect, increased production of lactic acid by the tumor [32] even in normoxia [18, 26, 28]. A qualitative study of the genetic deregulations at the cell scale would reveal how it impacts lactic-acid production to investigate the appearance of the Warburg effect. The primary aim of this study is to investigate the role of genetic regulations in cell metabolic changes.

In our mathematical model, the regulating effect of a gene on another is mainly driven by the γ parameter in the shifted-Hill function. Setting this parameter equal to 1 simulates a loss of the regulating function. An over-sensitivity of a gene by its regulator is modeled by setting the γ parameter to 40, the maximum defined in the model from [19]. Results of a few regulations are shown in Figure 3.

When no genetic deregulations are applied to the model (Figure 3A), protons production range from 0.0001 to 0.001 mmol/L/min with normal γ parameters. Around 0.01 mmol/L oxygen (1%), the cell progressively increases

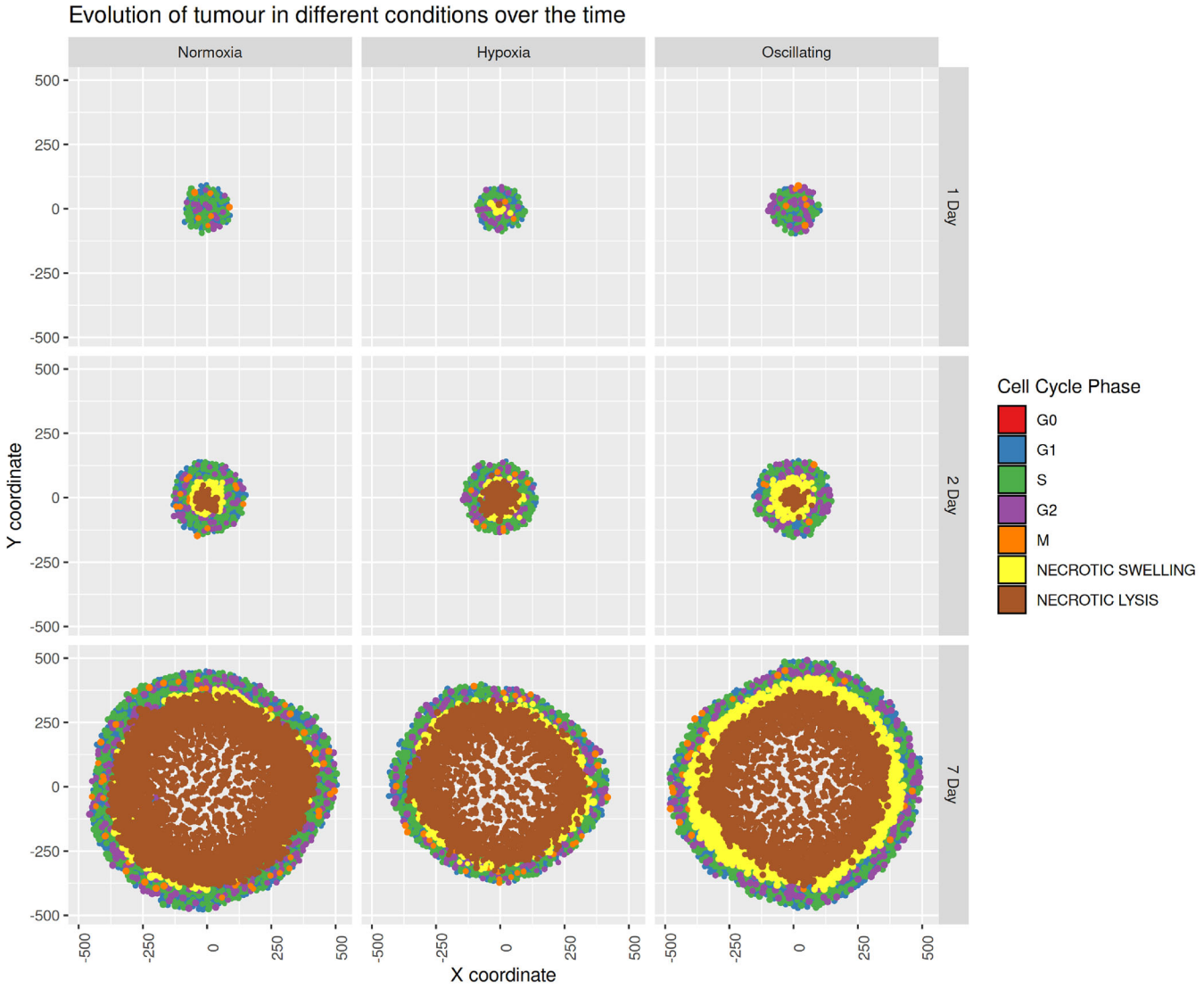

FIGURE 4 Evolution of tumor growth at different times in different conditions. In oscillating conditions, the oxygen concentration is slowly decreased from normoxia to hypoxia for 6 h, then cells are slowly put back in normoxia at the same rate. This process is repeated until the end of the simulation

its H^+secretion rate from 0.0001 mmol/L/min to the maximum of 0.001 mmol/L/min.

In our model, when HIF is not subjected to oxygen degradation (Figure 3B), the rate of H^+production is only influenced by the glucose concentration. In this case, cell's lactic acid secretion rate can reach 0.001 mmol/L/min even in normal oxygen pressure, as a result of the Warburg effect. Increased degradation of HIF in oxygen (Figure 3C) reduces the oxygen threshold at which the cell has a lactic acid secretion rate of 0.001 mmol/L/min. Lower levels of oxygen are needed to reach the maximal secretion rate compared to the normal degradation rate of HIF. With no deregulation (Figure 3A), the lactic acid secretion rate starts to increase at around 0.019 mmol/L of oxygen and reaches a maximum at around 0.08 mmol/L. With increased HIF degradation by oxygen (Figure 3C), this span is reduced and lactic-acid secretion increases at around 0.012 mmol/L of oxygen. Similar to our result, a model from [15] shows that a lower degradation rate of HIF increases the chance that cells use glycolysis instead of OXPHOS, which will increase lactic acid secretions.

Inhibiting LDH sensitivity to HIF (Figure 3D) causes the maximum lactic acid secretion rate to fall to 0.0008 mmol/L/min. Increasing LDH sensitivity to HIF does not permit the cell to have a higher H^+production rate in normoxia, while a decrease prevents a high H^+production rate in hypoxia (results not shown).

Interfering with PDK sensitivity to HIF or PDH sensitivity to PDK seems to have no effect on acid production in the model but on oxygen consumption by the cell (results not shown).

3.2 | Exploration of environment and genetic properties on the emergence of the Warburg phenotype

3.2.1 | Influence of environmental oxygen conditions

The Warburg effect is currently defined as the high production of acidity due to the use of glycolysis even in normoxia [7, 8, 15]. We ran several simulations with different environmental oxygen conditions to assess whether microenvironmental conditions only can induce a Warburg effect in the model.

Figure 4 shows how oxygen conditions affect tumor growth. In oscillating conditions, the oxygen concentration varies between physiological normoxia and pathological hypoxia and reverses every 6 h until the end of the simulation. Kinetics of HIF show a peak after 6 h and a decrease to an equilibrium state after 24–48 h. We choose to simulate a 6 h-period of hypoxia/normoxia to avoid the cell reaching an equilibrium and to simulate stressful conditions with a high response to a low level of oxygen. Constant hypoxia slows down tumor growth and reduces tumor diameter compared to normoxia. In all 3 different conditions, the center of the tumor is composed of dead cells surrounded by living cells at the periphery. Only in normoxia and varying oxygen conditions, some cells in the center of the tumor do continue to divide (only visible after 7 days of growth). This may be due to the changes in the tumor microenvironment with the increased cell death at the center. As the cells die, more nutrients will be available to quiescent cells to enable them to renter proliferating phase. Moreover, spatial changes due to the shrinkage of dead cells can influence the availability of nutrients at the center. This might show a mechanism by which the tumor can grow back after a period of harsh conditions, for example, quiescence can be a mechanism to avoid drug's effect on the tumor cell [1]. The necrotic core has been observed in biological experiments run in the lab (Figure 5).

It seems that varying the concentration of oxygen from normoxia to hypoxia, and reversing this process, every 6 h does not affect the diameter of the tumor at the end of the simulation. However, a ring of necrotic cells in the swelling phase appears thicker than in other conditions.

Results in Figure 6 show acid production according to the extracellular oxygen concentration. The red line y-axis intercept is equal to 0.02085 mmol/L (2% O_2), which corresponds to the threshold of hypoxia in physiological conditions. It is the level at which HIF has a half-maximal response as well [23]. Cells above this level are considered to be in normoxia, while the rest of the cells are in hypoxia. Levels of extracellular oxygen fall below the hypoxia threshold after 2 days of growth in normoxic conditions (a necrotic core in the center of the tumor has already formed). Due to poor oxygen concentration, cells with higher glycolytic activity appear and reach and H^+production rate of almost 5×10^{-4}mmol/L/min. The maximum glycolytic activity of cells falls at 7 days of growth because of reduced glucose availability. When tumor growth is started in hypoxic conditions, high glycolytic activity is present after only 1 day of growth. In these conditions, the way the cell produces its energy is influenced only by glucose concentrations (similar to the result shown in Figure 3). Therefore, hypoxic conditions directly select cells with high glycolytic activity.

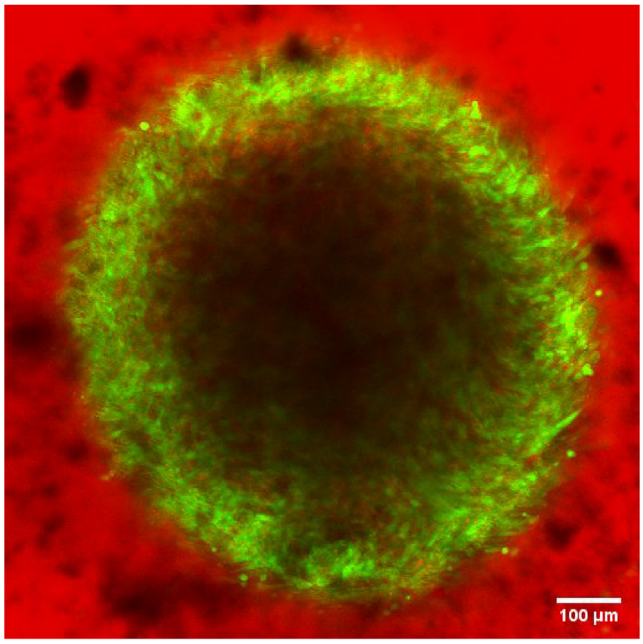

FIGURE 5 Picture of a spheroid grown for 30 days in an experiment run in the laboratory. Cells were marked using the fluorescent proteins Green FLuorescent Protein (GFP) and Sulforhodamine B (SRB). Living cells are colored in green, and dying cells appear in red. The center of the tumor is composed of hypoxic and dead cells, both do not emit fluorescence

The fact that, in the model, hypoxia may select cells with high glycolytic activity is supported by the levels of LDH/PDH genes presented in Figure 7. In normoxia, cells have a level of LDH and PDH of 1 for both; it can be associated with an oxidative state. In hypoxia, the LDH level reaches 3.0 and the PDH level falls to 0.25; it can be associated with a glycolytic state. At the beginning of the simulation in normoxic conditions, cells have 1:1 LDH/PDH levels. As the simulation goes on, oxygen becomes less available. Thus LDH level increases while PDH level decreases. The result in normoxic conditions shows that cells migrate from an oxidative to a glycolytic state as oxygen concentration decreases. Cells around 2:0.5 LDH/PDH levels have a hybrid state where

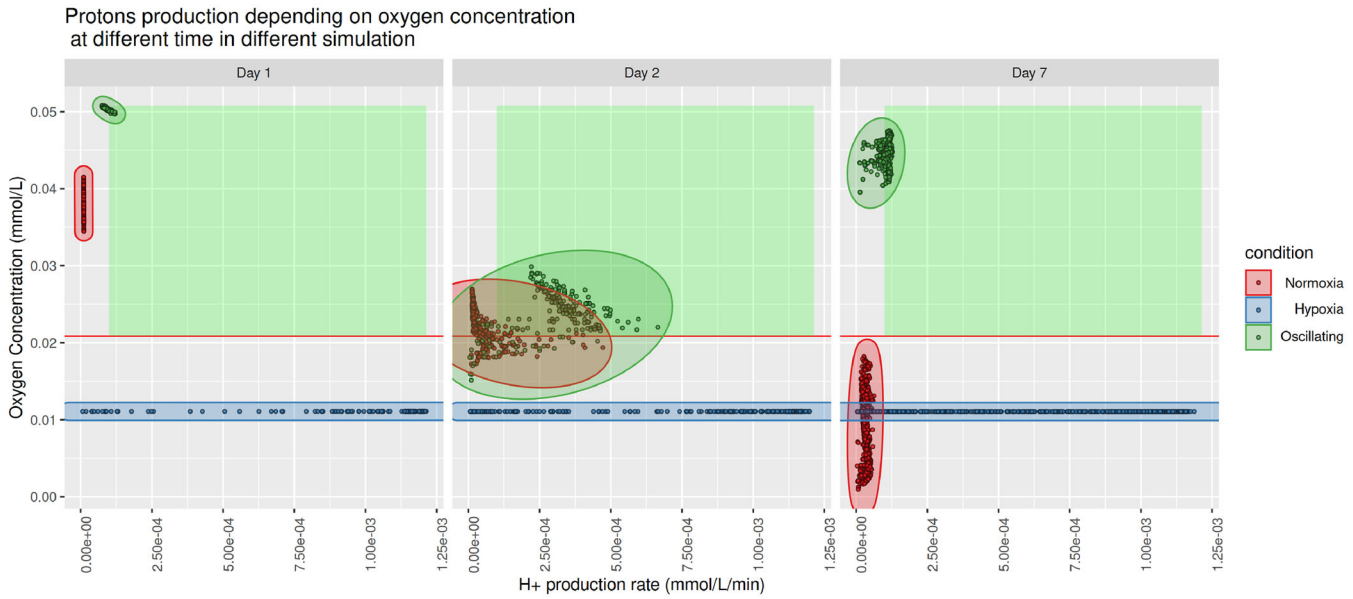

FIGURE 6 Acid production rate following oxygen extracellular concentrations at different times in different conditions. The red line indicates the hypoxia threshold. In oscillating conditions, the oxygen concentration is slowly decreased from normoxia to hypoxia during 6 h, then oxygen is increased to normoxia at the same rate. This process is repeated until the end of the simulation. Only living cells are represented on the graph. The green rectangle represents the region corresponding to a Warburg effect.

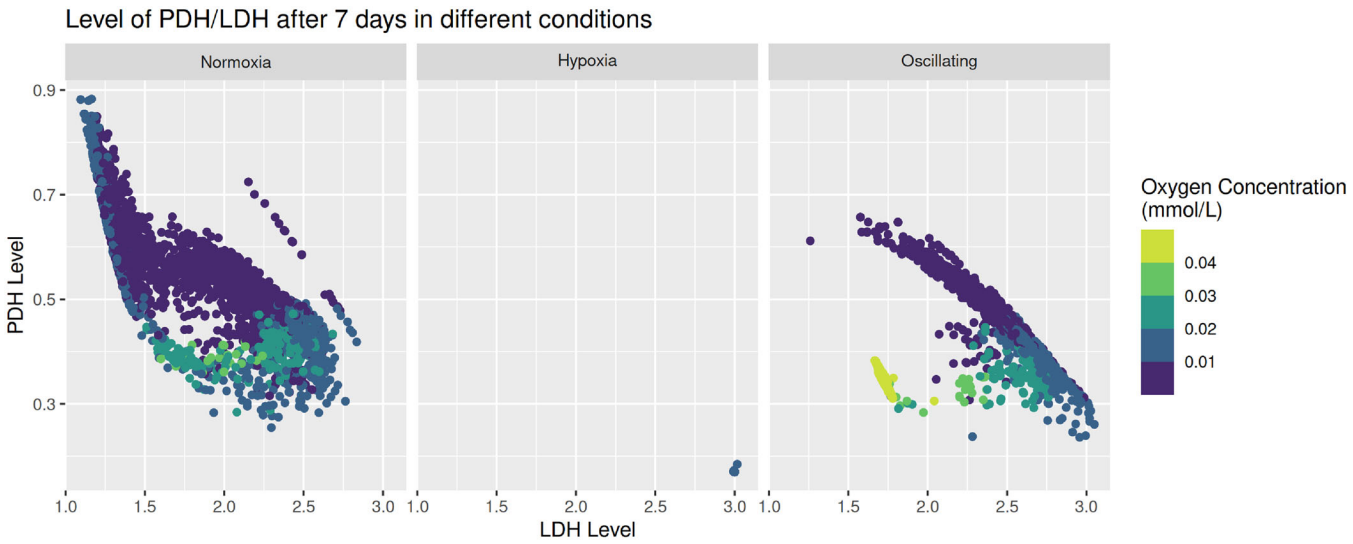

FIGURE 7 Plot of the level of PDH against the level of LDH colored by the extracellular oxygen concentration. The graph shows the results after 7 days of growth for different conditions. In oscillating conditions, the oxygen concentration is slowly decreased from normoxia to hypoxia during 6 h, then oxygen is increased to normoxia at the same rate. This process is repeated until the end of the simulation. Only living cells are represented on the graph

they rely on both nutrients to produce ATP. Again hypoxia selects for cells with high levels of LDH and low levels of PDH, suppressing the possibility for the cell to adopt a hybrid state.

Interestingly, the extracellular oxygen concentration after 7 days is higher when oxygen varies between normoxia and hypoxia every 6 h than in constant normoxia. Since cells are put in hypoxia several times a day, they rely more on glycolysis and consume less oxygen. Cells with higher glycolytic activity (2.5×10^{-4}mmol/L/min) even above the threshold of hypoxia appearing at 2 days. It suggests that the Warburg Effect can be caused by

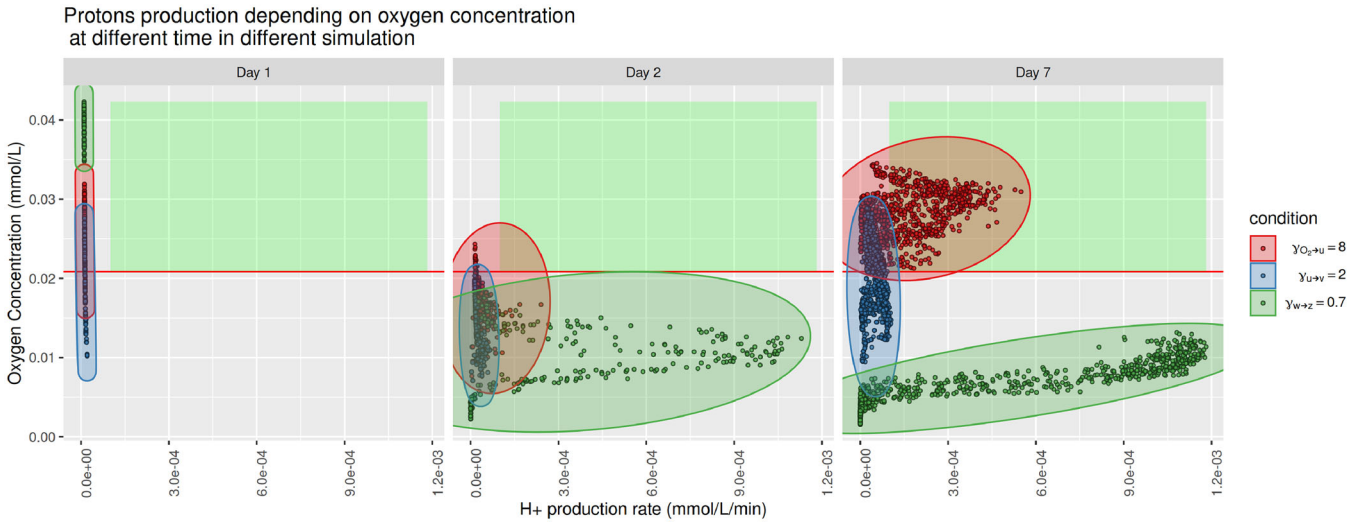

FIGURE 8 Acid production rate following oxygen extracellular concentrations at different times with different genetic perturbations. The red line indicates the hypoxia threshold. Only living cells are represented on the graph. Three genetic perturbations have been selected: reduced oxygen-induced degradation of HIF ($\gamma O_2 \rightarrow HIF = 8.0$), lower use of glycolysis in hypoxic conditions ($\gamma HIF \rightarrow LDH = 2.0$), and lower effect of hypoxia on oxygen consumption ($\gamma PDK \rightarrow PDH = 0.7$). Tumor growth was initiated in normoxia. The green rectangle represents the region corresponding to a Warburg effect

environmental conditions with rapid variations. Combined with Figure 7, genetic levels seem to indicate that cells cannot enter a complete oxidative state and are trapped either in a hybrid or a glycolytic state.

3.2.2 | Influence of the intrinsic genetic properties of the cell

Here, tumor growth is initiated in normoxia (results not shown). Extracellular oxygen concentrations only vary due to cell consumption and reduced diffusion in the tumor. Only genetic regulations have been modified between each simulation to assess the impact of different genetic deregulations (mutations or epigenetic alterations) on tumor growth and cell metabolism. Results are similar to normoxic conditions with no genetic deregulations (presented in Figure 4). When reducing inhibition of PDH by PDK, tumor radius at 7 days of growth is lower than in normoxia and higher than in hypoxia with no mutation.

Figure 8 shows that cells start to become hypoxic after day 1, reaching a majority by day 2. After 7 days with a reduced HIF degradation rate by oxygen, extracellular oxygen goes back to normoxic levels yet cells have a higher acid production rate that corresponds to a Warburg effect. In this case, we suppose that cells slowly drain oxygen levels in the environment to a point where hypoxia is reached. Due to poor oxygen conditions, cells adapt their metabolism to enter a glycolytic state that they keep even if the oxygen supply goes back above 2% O_2. Together with the result in Figure 9, this might be caused by a delay in the response from returning to normal conditions since HIF regulation by O_2 is affected. While some cells have levels of LDH greater than 2 and PDH lower than 0.50 (hybrid to glycolytic state), some have a ratio of LDH/PDH almost equal to 1:1. This suggests that the Warburg Effect is not irreversible with a reduced HIF degradation rate by oxygen alone.

As expected, reducing the increase in LDH levels due to HIF response does not induce a high acidification rate in normoxia but affects the maximum acid production rate and level of LDH. Instead of inducing a glycolytic phenotype, it seems to repress it.

Reducing the inhibiting power of PDK on PDH allows the cell to keep a higher PDH level, a key enzyme for oxygen consumption and oxidative state in the model. Cells exhibit an acid production rate similar to those in hypoxic conditions after 2 and 7 days, compared to other genetics deregulation. While in normoxia with no genetic deregulation cells seem to fluctuate around the threshold of hypoxia, here they are all below this level. Since PDH is not effectively regulated by HIF, the cell tends to stay in an oxidative state and rely less on glycolysis. We can suppose that cells consume oxygen even when the level fall, creating further harder conditions. Results also show that adaptation to hypoxia is delayed, and the cell only adopts a glycolytic state at oxygen conditions near-pathological hypoxia. PDH levels do not fall far below 0.75 even after 7 days of growth compared to other conditions, indicating that cells can only adopt an oxidative or hybrid state.

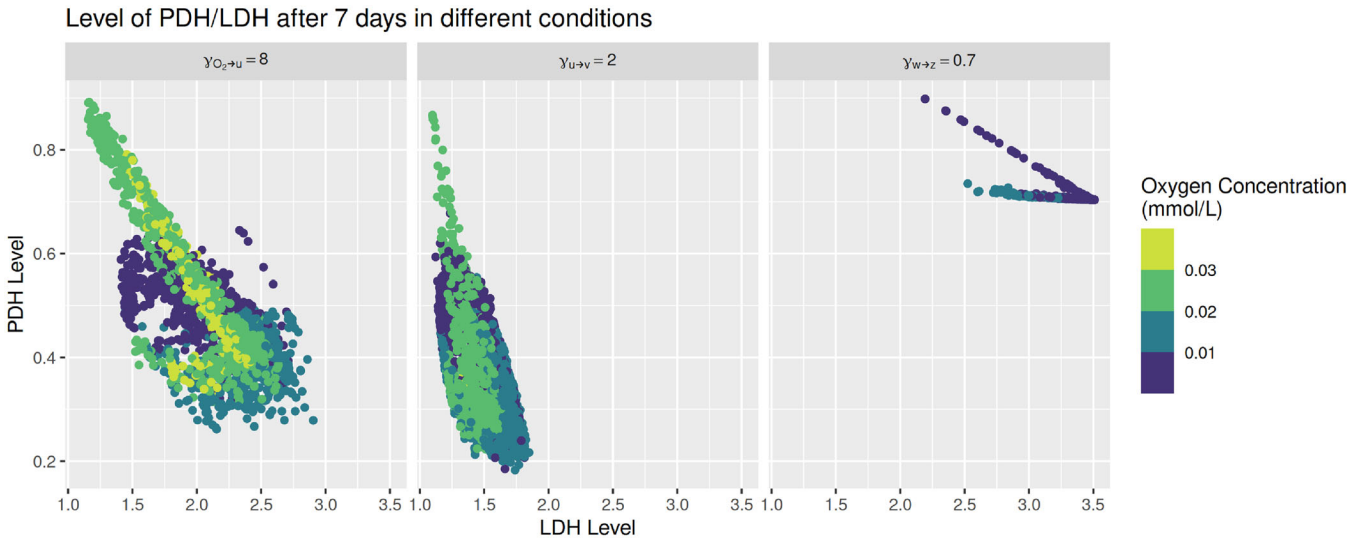

FIGURE 9 Plot of the level of PDH against the level of LDH colored by the extracellular oxygen concentration. The graph shows the results after 7 days of growth with three different genetic perturbations: reduced oxygen-induced degradation of HIF ($\gamma O_2 \to HIF = 8.0$), lower use of glycolysis in hypoxic conditions ($\gamma HIF \to LDH = 2.0$) and lower effect of hypoxia on the oxygen consumption ($\gamma PDK \to PDH = 0.7$). Tumor growth was initiated in normoxia

4 | DISCUSSION

In this paper, we formulated a mathematical model to study the impact of HIF on LDH and PDH, key enzymes of glycolysis and TCA cycle and thus investigating its role in cellular metabolism. Since its discovery, HIF has been actively studied by the scientific community. There are several modeling approaches to study the effects of HIF [2, 15, 19, 25], and here we investigate its role using a multiagent model, considering a heterogeneous environment that changes over time. Furthermore, the model is used to investigate the impact of genes on metabolism and the effect of different environmental conditions and different genetic deregulations (such as mutations or epigenetic alterations) can have on the Warburg effect, an overproduction of acidity due to an increase in glycolysis even in normoxia. Overproduction of lactate can also be caused by reduced use of pyruvate in the mitochondria, remaining pyruvate is then turned into lactate.

Using the level of LDH and PDH genes as markers, we can define three different metabolic states [15, 19] such as oxidative, glycolytic, and hybrid. The oxidative state corresponds to a high level of PDH and a low level of LDH and inversely to a glycolytic state. The hybrid state then corresponds to medium levels of both enzymes, 2:0.5 for LDH and PDH, respectively. As expected, normoxia strongly selects for the first state while hypoxia selects for the second one. The hybrid state is observed as the oxygen levels change over time due to tumor growth. Thus it appears that the cell adopts this state when adapting to changing oxygen conditions or when oxygen levels vary between normoxia and hypoxia several times during tumor growth (oscillating conditions in the model).

We observed some differences between our model and the model in a recent paper from Li et al. [19]: (1) they identified a normal state with a level of LDH at 1 and a level of PDH at 0.1, and (2) their oxidative and glycolytic states have different levels of genes than those present in our model. This difference in the result can be explained by the fact that we only include a small fraction of their gene regulation network in our model, to only account for the effect caused by HIF.

We have simulated tumor growth when oxygen supply does not vary over time; hence, differences in extracellular oxygen level can only be caused by cell consumption or reduced diffusion owing to higher cell density. We found that when there are rapid changes in oxygen supply to the tumor, cells with higher glycolytic rates above the threshold of hypoxia appear. It shows that varying microenvironmental conditions are sufficient to induce a Warburg phenotype for the cell. The results are in line with the findings by Damaghi et al. [8]. However, the model does not include sudden genetic mutation which can be caused by harsh conditions. Therefore, in our case cell would not be trapped into a Warburg phenotype and this state can be reversed to a normal state if the cell is given enough time in favorable conditions. Lactate secretion, which decreases the extracellular pH, depends on glucose consumption. A study by Casciari et al. [5] has shown that a lower extracellular pH decreases dramatically glucose consumption, and the Warburg effect could also be inhibited by low pH (6.95). We may suppose that after difficult

conditions genes may be overexpressed or inhibited which will force the cell to adopt a Warburg phenotype.

The importance of HIF degradation in normoxia is further highlighted by the model results. We were also able to induce a Warburg effect by reducing the degradation rate of HIF by oxygen-dependent enzymes. Our results show that this effect only appears after the first period of hypoxia. It suggests that HIF accumulation forces the cell to adopt a glycolytic state and prevents it from returning to an oxidative state in normoxia. HIF inhibition therapy would prevent the appearance of Warburg cell type in cancer. PI3K and mTOR, two genes that increase HIF level independently of the level of oxygen [12, 17, 22], are studied as potential targets in anticancer therapy due to their altered expression in cancer and their role in signaling pathways affecting many biological functions [31, 35], possibly causing HIF overexpression. AMP-activated protein kinase (AMPK) enzyme is known to interact with HIF [15] and inhibits its expression, and some evidence links this gene to anti-tumor activity [20]. These interactions could be added in further modeling work to study their impact on the Warburg effect as they may be important players interacting with HIF.

It has been shown that extracellular pH can (1) influence the cell metabolism (reduce glucose consumption, increase the cells doubling time) [5]; (2) affect the ability of tumor cells to form metastasis, invade other tissue, or migrate [33]; and (3) could be a mechanism of invasion [29]. Currently, therapy targeting extracellular pH in the tumor is under development. Moreover, pH also affects the efficiency of different drugs such as temozolomide [30]. Reducing the increase in the LDH level by the cell response to hypoxia lowered the rate of acid production in our simulation. Inhibitors of LDH could be used in combination with pH-targeting therapy to improve treatment outcomes.

Reducing the downregulation of PDH by HIF in the model forces the cell to rely as much as possible on oxygen to produce its energy. Herein, changes in metabolism toward glycolytic activity require lower levels of oxygen. A study has shown that inhibition of HIF resulted in reduced lactate production, an increase in oxygen consumption, and radiotherapy sensitivity [18]. Whether increasing oxygen consumption by PDH upregulation would result in better outcomes in therapy in the model remains to be studied.

ACKNOWLEDGMENTS

We thank Alaa Tafech for providing the picture of the spheroid in Figure 5. This project has received financial support from CNRS through the MITI interdisciplinary programs. Kévin Spinicci gratefully acknowledges the support of Swansea University Strategic Partnership Research Scholarship and the support of IDEX Université Grenoble Alpes.

CONFLICTS OF INTEREST

The authors declare no conflict of interest.

DATA AVAILABILITY STATEMENT

The authors declare no data availabity statement.

ORCID

Kévin Spinicci https://orcid.org/0000-0001-9200-4401

REFERENCES

1. T. Alarcón and H. J. Jensen, *Quiescence: A mechanism for escaping the effects of drug on cell populations*, J. R. Soc. Interf. **8** (2011), no. 54, 99–106. https://doi.org/10.1098/rsif.2010.0130.
2. B. Bedessem and A. Stéphanou, *A mathematical model of HiF-1α-mediated response to hypoxia on the G1/S transition*, Math. Biosci. **248** (2014), no. 1, 31–39. https://doi.org/10.1016/j.mbs.2013.11.007.
3. R. A. Bender, Glycolysis, *Brenner's Encyclopedia of Genetics*, 2nd ed, **2** (2013), 346–349. https://doi.org/10.1016/B978-0-12-374984-0.00659-8.
4. A. Blanco and G. Blanco, *Medical biochemistry*. Academic Press, New York, 2018, pp. 283–323, 2017. https://doi.org/10.1016/B978-0-12-803550-4/00014-8.
5. J. J. Casciari, S. V. Sotirchos, and R. M. Sutherland, *Variations in tumor cell growth rates and metabolism with oxygen concentration, glucose concentration, and extracellular pH*, J. Cell. Physiol. **151** (1992), no. 2, 386–394. https://doi.org/10.1002/jcp.1041510220.
6. G. M. Cooper, *The eukaryotic cell cycle*. 2000. https://www.ncbi.nlm.nih.gov/books/NBK9876/.
7. R. Courtnay, D. C. Ngo, N. Malik, K. Ververis, S. M. Tortorella, and T. C. Karagiannis, *Cancer metabolism and the Warburg effect: the role of HIF-1 and PI3K*, Mol. Biol. Rep. **42** (2015), no. 4, 841–851. https://doi.org/10.1007/s11033-015-3858-x.
8. M. Damaghi, J. West, M. Robertson-Tessi, L. Xu, M. Ferrall-Fairbanks, P. Stewart, E. Persi, B. Fridley, P. Altrock, R. Gatenby, P. Sims, A. Anderson, and R. Gillies, *The harsh microenvironment in early breast cancer selects for a Warburg phenotype*, bioRxiv (2020), 2020.04.07.029975. https://doi.org/10.1101/2020.04.07.029975.
9. A. Ghaffarizadeh, R. Heiland, S. H. Friedman, S. M. Mumenthaler, and P. Macklin, *PhysiCell: An open source physics-based cell simulator for 3-D multicellular systems*, PLoS Comput. Biol. **14** (2018), no. 2, e1005991. https://journals.plos.org/ploscompbiol/article?id=10.1371/journal.pcbi.1005991.
10. N. Goda, S. J. Dozier, and R. S. Johnson, *HIF-1 in cell cycle regulation, apoptosis, and tumor progression*, Antioxid Redox Signal. **5** (2003), 467–473. https://www.liebertpub.com/doi/abs/10.1089/152308603768295212.
11. C. Granchi, S. Bertini, M. Macchia, and F. Minutolo, *Inhibitors of lactate dehydrogenase isoforms and their therapeutic potentials*, Curr. Med. Chem. **17** (2010), no. 7, 672–697. https://pubmed.ncbi.nlm.nih.gov/20088761/.
12. Y. Hayashi, A. Yokota, H. Harada, and G. Huang, *Hypoxia/pseudohypoxia-mediated activation of hypoxia-*

inducible factor-1α in cancer, Cancer Sci. **110** (2019), no. 5, 1510–1517. https://onlinelibrary.wiley.com/doi/abs/10.1111/cas.13990.

13. S. Heydarzadeh, A. A. Moshtaghie, M. Daneshpoor, and M. Hedayati, *Regulators of glucose uptake in thyroid cancer cell lines*, Cell Commun. Signal. **18** (2020), 83. https://doi.org/10.1186/s12964-020-00586-x.
14. P. Jacquet and A. Stéphanou, *Metabolic reprogramming, questioning, and implications for cancer*, Biology **10** (2021), no. 2, 129. https://www.mdpi.com/2079-7737/10/2/129/.
15. D. Jia, M. Lu, K. H. Jung, J. H. Park, L. Yu, J. N. Onuchic, B. A. Kaipparettu, and H. Levine, *Elucidating cancer metabolic plasticity by coupling gene regulation with metabolic pathways*, PNAS **116** (2019), no. 9, 3909–3918. https://pubmed.ncbi.nlm.nih.gov/30733294/.
16. T. C. King, Cell injury, cellular responses to injury, and cell death, *Elsevier's Integrated Pathology* (2007), 1–20. https://doi.org/10.1016/b978-0-323-04328-1.50007-3.
17. J.-W. Lee, S.-H. Bae, J.-W. Jeong, S.-H. S.-H. K. Kim, and K.-W. Kim., *Hypoxia-inducible factor (HIF -1)alpha : its protein stability and biological functions*, Exp. Mol. Med. **36** (2004), no. 1, 1–12. https://www.nature.com/articles/emm20041.
18. E. Leung, R. A. Cairns, N. Chaudary, R. N. Vellanki, T. Kalliomaki, E. H. Moriyama, H. Mujcic, B. C. Wilson, B. G. Wouters, R. Hill, and M. Milosevic, *Metabolic targeting of HIF-dependent glycolysis reduces lactate, increases oxygen consumption and enhances response to high-dose single-fraction radiotherapy in hypoxic solid tumors*, BMC Cancer **17** (2017), no. 1, 418. https://bmccancer.biomedcentral.com/articles/10.1186/s12885-017-3402-6.
19. W. Li and J. Wang, *Uncovering the underlying mechanisms of cancer metabolism through the landscapes and probability flux quantifications*, iScience **23** (2020), no. 4, 101002. https://doi.org/10.1016/j.isci.2020.101002.
20. W. Li, S. M. Saud, M. R. Young, G. Chen, and B. Hua, *Targeting AMPK for cancer prevention and treatment*. Oncotarget **6** (2015), no. 10, 73657378. https://doi.org/10.18632/oncotarget.3629.
21. A. Marin-Hernandez, J. Gallardo-Perez, S. Ralph, S. Rodriguez-Enriquez, and R. Moreno-Sanchez, *HIF-1alpha modulates energy metabolism in cancer cells by inducing over-expression of specific glycolytic isoforms*, Mini Rev. Med. Chem. **9** (2009), no. 9, 1084–1101. http://www.eurekaselect.com/openurl/content.php?genre=article&issn=1389-5575&volume=9&issue=9&spage=1084.
22. G. N. Masoud and W. Li, *HIF-1α pathway: Role, regulation and intervention for cancer therapy*, Acta Pharmaceutica Sinica B **5** (2015), no. 5, 378–389. https://www.sciencedirect.com/science/article/pii/S2211383515000817?pes=vor.
23. S. R. McKeown, *Defining normoxia, physoxia and hypoxia in tumours - Implications for treatment response*, Br. J. Radiol. **87** (2014), 20130676. https://pmc/articles/PMC4064601/%20/pmc/articles/PMC4064601/?report=abstract%20https://www.ncbi.nlm.nih.gov/pmc/articles/PMC4064601/.
24. R. McLendon, A. Friedman, D. Bigner, E. G. Van Meir, D. J. Brat, G. M. Mastrogianakis, J. J. Olson, T. Mikkelsen, N. Lehman, K. Aldape, W. K. Yung, O. Bogler, J. N. Weinstein, S. VandenBerg, M. Berger, M. Prados, D. Muzny, M. Morgan, S. Scherer, A. Sabo, L. Nazareth, L. Lewis, O. Hall, Y. Zhu, Y. Ren, O. Alvi, J. Yao, A. Hawes, S. Jhangiani, G. Fowler, A. San Lucas, C. Kovar, A. Cree, H. Dinh, J. Santibanez, V. Joshi, M. L. Gonzalez-Garay, C. A. Miller, A. Milosavljevic, L. Donehower, D. A. Wheeler, R. A. Gibbs, K. Cibulskis, C. Sougnez, T. Fennell, S. Mahan, J. Wilkinson, L. Ziaugra, R. Onofrio, T. Bloom, R. Nicol, K. Ardlie, J. Baldwin, S. Gabriel, E. S. Lander, L. Ding, R. S. Fulton, M. D. McLellan, J. Wallis, D. E. Larson, X. Shi, R. Abbott, L. Fulton, K. Chen, D. C. Koboldt, M. C. Wendl, R. Meyer, Y. Tang, L. Lin, J. R. Osborne, B. H. Dunford-Shore, T. L. Miner, K. Delehaunty, C. Markovic, G. Swift, W. Courtney, C. Pohl, S. Abbott, A. Hawkins, S. Leong, C. Haipek, H. Schmidt, M. Wiechert, T. Vickery, S. Scott, D. J. Dooling, A. Chinwalla, G. M. Weinstock, E. R. Mardis, R. K. Wilson, G. Getz, W. Winckler, R. G. Verhaak, M. S. Lawrence, M. O'Kelly, J. Robinson, G. Alexe, R. Beroukhim, S. Carter, D. Chiang, J. Gould, S. Gupta, J. Korn, C. Mermel, J. Mesirov, S. Monti, H. Nguyen, M. Parkin, M. Reich, N. Stransky, B. A. Weir, L. Garraway, T. Golub, M. Meyerson, L. Chin, A. Protopopov, J. Zhang, I. Perna, S. Aronson, N. Sathiamoorthy, G. Ren, J. Yao, W. R. Wiedemeyer, H. Kim, W. K. Sek, Y. Xiao, I. S. Kohane, J. Seidman, P. J. Park, R. Kucherlapati, P. W. Laird, L. Cope, J. G. Herman, D. J. Weisenberger, F. Pan, D. Van Den Berg, L. Van Neste, M. Y. Joo, K. E. Schuebel, S. B. Baylin, D. M. Absher, J. Z. Li, A. Southwick, S. Brady, A. Aggarwal, T. Chung, G. Sherlock, J. D. Brooks, R. M. Myers, P. T. Spellman, E. Purdom, L. R. Jakkula, A. V. Lapuk, H. Marr, S. Dorton, G. C. Yoon, J. Han, A. Ray, V. Wang, S. Durinck, M. Robinson, N. J. Wang, K. Vranizan, V. Peng, E. Van Name, G. V. Fontenay, J. Ngai, J. G. Conboy, B. Parvin, H. S. Feiler, T. P. Speed, J. W. Gray, C. Brennan, N. D. Socci, A. Olshen, B. S. Taylor, A. Lash, N. Schultz, B. Reva, Y. Antipin, A. Stukalov, B. Gross, E. Cerami, Q. W. Wei, L. X. Qin, V. E. Seshan, L. Villafania, M. Cavatore, L. Borsu, A. Viale, W. Gerald, C. Sander, M. Ladanyi, C. M. Perou, D. N. Hayes, M. D. Topal, K. A. Hoadley, Y. Qi, S. Balu, Y. Shi, J. Wu, R. Penny, M. Bittner, T. Shelton, E. Lenkiewicz, S. Morris, D. Beasley, S. Sanders, A. Kahn, R. Sfeir, J. Chen, D. Nassau, L. Feng, E. Hickey, A. Barker, D. S. Gerhard, J. Vockley, C. Compton, J. Vaught, P. Fielding, M. L. Ferguson, C. Schaefer, J. Zhang, S. Madhavan, K. H. Buetow, F. Collins, P. Good, M. Guyer, B. Ozenberger, J. Peterson, and E. Thomson, *Comprehensive genomic characterization defines human glioblastoma genes and core pathways*, Nature **455** (2008), no. 7216, 1061–1068. https://www.nature.com/articles/nature07385.
25. M. Robertson-Tessi, R. J. Gillies, R. A. Gatenby, and A. R. Anderson, *Impact of metabolic heterogeneity on tumor growth, invasion, and treatment outcomes*, Cancer Res. **75** (2019), no. 8, 1567–1579. http://cancerres.aacrjournals.org/lookup/doi/10.1158/0008-5472.CAN-14-1428.
26. I. F. Robey, A. D. Lien, S. J. Welsh, B. K. Baggett, and R. J. Gillies, *Hypoxia-inducible factor-1α and the glycolytic phenotype in tumors*, Neoplasia **7** (2005), no. 4, 324–330. https://doi.org/10.1593/neo.04430.
27. L. Slemc and T. Kunej, *Transcription factor HIF1A: downstream targets, associated pathways, polymorphic hypoxia response element (HRE) sites, and initiative for standardization of reporting in scientific literature*, Tumor Biol. **37** (2016), no. 11, 14851–14861. https://doi.org/10.1007/s13277-016-5331-4.
28. K. Smallbone, R. A. Gatenby, R. J. Gillies, P. K. Maini, and D. J. Gavaghan, *Metabolic changes during carcinogenesis: potential impact on invasiveness*, J. Theor. Biol. **244** (2007), no. 4, 703–713. https://doi.org/10.1016/J.JTBI.2006.09.010.

29. K. Smallbone, R. A. Gatenby, and P. K. Maini, *Mathematical modelling of tumour acidity*, J. Theor. Biol. **255** (2008), no. 1, 106–112. https://doi.org/10.1016/j.jtbi.2008.08.002.
30. A. Stéphanou and A. Ballesta, *pH as a potential therapeutic target to improve temozolomide antitumor efficacy : A mechanistic modeling study*, Pharmacol. Res. Perspect. **7** (2019), no. 1. https://doi.org/10.1002/PRP2.454.
31. T. Tian, X. Li, and J. Zhang, *mTOR signaling in cancer and mTOR inhibitors in solid tumor targeting therapy*, Int. J. Mol. Sci. **20** (2019), 755.
32. O. Warburg, F. Wind, and E. Negelein, *The metabolism of tumors in the body*, J. Gen. Physiol. **8** (1927), no. 6, 519–530. https://doi.org/10.1085/jgp.8.6.519.
33. S. D. Webb, J. A. Sherratt, and R. G. Fish, *Mathematical modelling of tumor acidity: regulation of intracellular pH*, J. Theor. Biol. **196** (1999), no. 2, 237–250. https://doi.org/10.1006/JTBI.1998.0836.
34. J. Xu, B. Wang, Y. Xu, L. Sun, W. Tian, D. Shukla, R. Barod, J. Grillari, R. Grillari-Voglauer, P. H. Maxwell, and M. A. Esteban, *Epigenetic regulation of HIF-1α in renal cancer cells involves HIF-1α/2α binding to a reverse hypoxia-response element*, Oncogene **31** (2012), no. 8, 1065–1072. https://doi.org/10.1038/onc.2011.305.
35. J. Yang, J. Nie, X. Ma, Y. Wei, Y. Peng, and X. Wei, *Targeting PI3K in cancer: Mechanisms and advances in clinical trials*, Mol. Cancer **18** (2019), 26.
36. J. J. Zimmerman, A. von Saint André-von Arnim, and J. McLaughlin, *Cellular respiration*, 4th ed, Elsevier, Amsterdam, 2011. http://doi.org/10.1016/B978-0-323-07307-3.10074-6.
37. F. K. Zimmermann, Glycolysis in Saccharomyces cerevisiae, *Encyclopedia of Genetics* (2001), 885–888. https://doi.org/10.1006/rwgn.2001.0570.

SUPPORTING INFORMATION

Additional supporting information can be found online in the Supporting Information section at the end of this article.

How to cite this article: K. Spinicci, P. Jacquet, G. Powathil, and A. Stéphanou, *Modeling the role of HIF in the regulation of metabolic key genes LDH and PDH: Emergence of Warburg phenotype*, Comp. Sys. Onco. **2** (2022), e1040. https://doi.org/10.1002/cso2.1040